

Supporting Information (SI)

Improved Cycling Stability in High-Capacity Li-rich Vanadium containing Disordered Rock Salt Oxyfluoride Cathodes

Christian Baur,^{a*} Ida Källquist,^b Johann Chable,^a Jin Hyun Chang,^c Rune E. Johnsen,^c Francisco Ruiz-Zepeda,^d Jean-Marcel Ateba Mba,^d Andrew J. Naylor,^e Juan Maria García-Lastra,^c Tejs Vegge,^c Franziska Klein,^a Annika R. Schür,^a Poul Norby,^c Kristina Edström,^e Maria Hahlin,^b and Maximilian Fichtner,^{a,f}

a Helmholtz Institute Ulm for Electrochemical Energy Storage, Helmholtzstraße 11, 89081 Ulm, Germany.

b Uppsala University, Department of Physics and Astronomy, P.O. Box 256, SE-751 05 Uppsala, Sweden

c Technical University of Denmark, Department of Energy Conversion and Storage, 2800 Kgs. Lyngby, Denmark.

d National Institute of Chemistry, Hajdrihova 19, P.O. Box 660, SI-1000 Ljubljana, Slovenia.

e Department of Chemistry - Ångström Laboratory, Uppsala University, Box 538, 75121 Uppsala, Sweden

f Institute of Nanotechnology, Karlsruhe Institute for Technology, P.O. Box 3640, 76021 Karlsruhe, Germany.

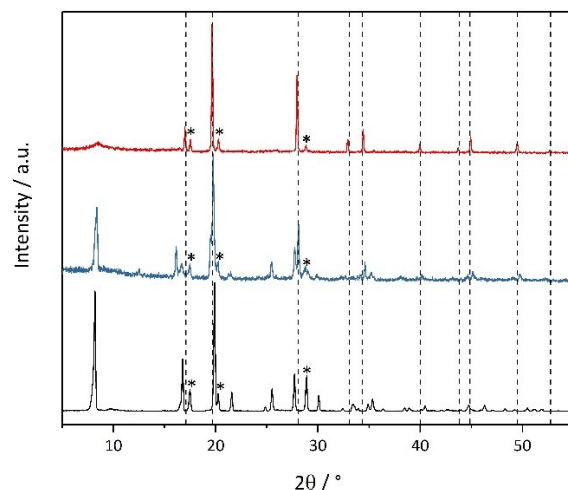
Supporting note 1 – Ceramic synthesis approach of disordered rock salt oxyfluorides

$\text{Li}_2\text{VO}_2\text{F}$ and similar DRS oxyfluorides have so far only been synthesized by using high energy ball milling techniques. The reason may originate from the metastability of the DRS phase and the inaccessibility of such phases with conventional synthesis techniques. We tried several approaches following a conventional ceramic synthesis approach to synthesize $\text{Li}_2\text{VO}_2\text{F}$, but these did not yield the DRS phase (Figure S1). However, when substituting 50% of the V_2O_3 precursor with the corresponding isovalent Ti^{3+} or Fe^{3+} oxide, the ceramic synthesis approach yields materials consisting partially of the DRS phase with residual LiF left (Figure S1). This indicates that the TM substitution increases the thermodynamic stability of the DRS phase, which enabling the accessibility of the phase ($\text{Li}_{1+x}\text{TM}'_y\text{TM}''_{1-y}\text{O}_2\text{F}_x$; $x < 1$; $y = 0.5$; $\text{TM}' = \text{V}^{3+}$; $\text{TM}'' = \text{Fe}^{3+}$ or Ti^{3+}). In fact, both LiFeO_2 and LiTiO_2 with a DRS structure do exist.¹²

For the ceramic synthesis approach the precursors Li_2O (Alfa Aesar, 99.7%), LiF (Alfa Aesar, 99.9%) and the corresponding TM_2O_3 precursor (V_2O_3 (Alfa Aesar, 99.7%), Ti_2O_3 (Alfa Aesar, 99.8%) and Fe_2O_3 (Alfa Aesar, 99.9%)), were thoroughly ground in stoichiometric amounts in a mortar inside an argon-filled glovebox with water and oxygen levels below 0.1 ppm. Pellets of 100 mg were pressed using a Specac mini lab press. A pressure of two tons was applied to the pellet and kept for one minute. The pellets were transferred into stainless steel reactors and sealed. The samples were annealed at 850°C in a furnace for 1 h. After cooling down, the reactors were transferred back into a glovebox. The annealed pellets were ground in a mortar for 15 minutes and the obtained powder was used without further purification.

¹T. A. Hewston, B. L. Chamberland, *J. Phys. Chem. Solids* **1987**, *48*, 97–108.

²A. Urban, A. Abdellahi, S. Dacek, N. Artrith, G. Ceder, *Phys. Rev. Lett.* **2017**, *119*, 1–6.



Supporting Information Figure S1: Comparison of PXRD pattern (Mo $K_{\alpha 1}$) of synthesis attempts with a conventional ceramic synthesis using Li_2O , the corresponding TM_2O_3 and LiF in stoichiometric amounts. Black: resulting PXRD pattern of $\text{Li}_2\text{VO}_2\text{F}$ synthesis approach, blue: resulting PXRD pattern of $\text{Li}_2\text{V}_{0.5}\text{Ti}_{0.5}\text{O}_2\text{F}$ synthesis approach, red: resulting PXRD pattern of $\text{Li}_2\text{V}_{0.5}\text{Fe}_{0.5}\text{O}_2\text{F}$ synthesis approach. Black dotted lines schematically indicate position of the DRS phase ($Fm\bar{3}m$). Asterisk indicate LiF .

Supporting Information Table S1: Structural parameters of $\text{Li}_2\text{VO}_2\text{F}$, $\text{Li}_2\text{V}_{0.5}\text{Ti}_{0.5}\text{O}_2\text{F}$ and $\text{Li}_2\text{V}_{0.5}\text{Fe}_{0.5}\text{O}_2\text{F}$ obtained by the Rietveld

Compound		$\text{Li}_2\text{VO}_2\text{F}$	$\text{Li}_2\text{V}_{0.5}\text{Ti}_{0.5}\text{O}_2\text{F}$	$\text{Li}_2\text{V}_{0.5}\text{Fe}_{0.5}\text{O}_2\text{F}$
Space group		$Fm\bar{3}m$		
GoF		4.2583	3.9933	4.7164
R_p		1.2955	1.2758	1.6528
R_{wp}		1.6173	1.7917	2.1282
R_{Bragg}		1.1729	1.5000	1.4147
4a Wyckoff site	$B_{iso} / \text{\AA}^2$	1.05(3)	0.92(4)	0.94(4)
$x, y, z = (0, 0, 0)$	(cations)			
4b Wyckoff site	$B_{iso} / \text{\AA}^2$	1.29(4)	1.66(6)	1.75(6)
$x, y, z = (0.5, 0.5, 0.5)$	(anions)			
4a Wyckoff site	Occupancy TM	0.345(3)	0.325(6)	0.330(4)
$x, y, z = (0, 0, 0)$	Occupancy Li	0.655(3)	0.675(6)	0.670(4)
Size / nm		14.15	12.35	12.68
Strain / %		0.59	0.58	0.50
$a / \text{\AA}$		4.1169(4)	4.1342(6)	4.1388(6)
Volume / \AA^3		69.78(2)	70.66(3)	70.90(3)
Phase density / g cm^{-3}		3.73(2)	3.55(3)	3.68(2)

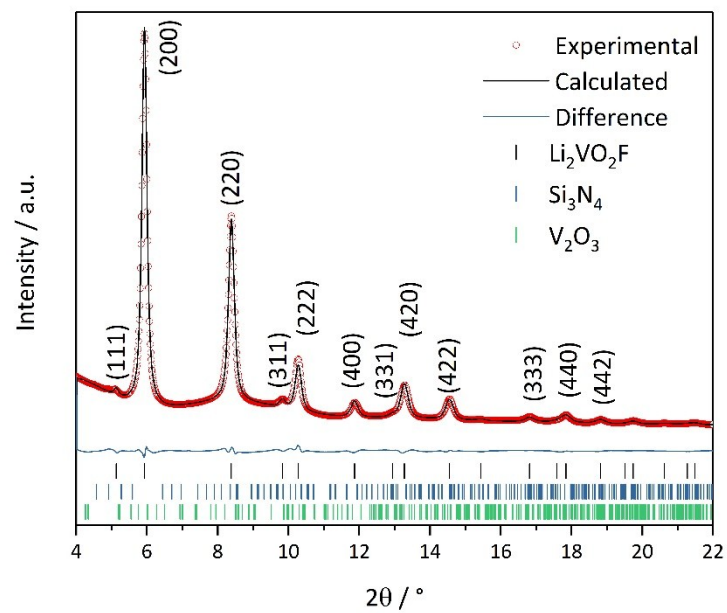
refinements.

*occupancy of anions was not refined and was set to 2/3 for O and 1/3 for F, respectively. The TM and Li occupancies were restrained to result in 1 and refined.

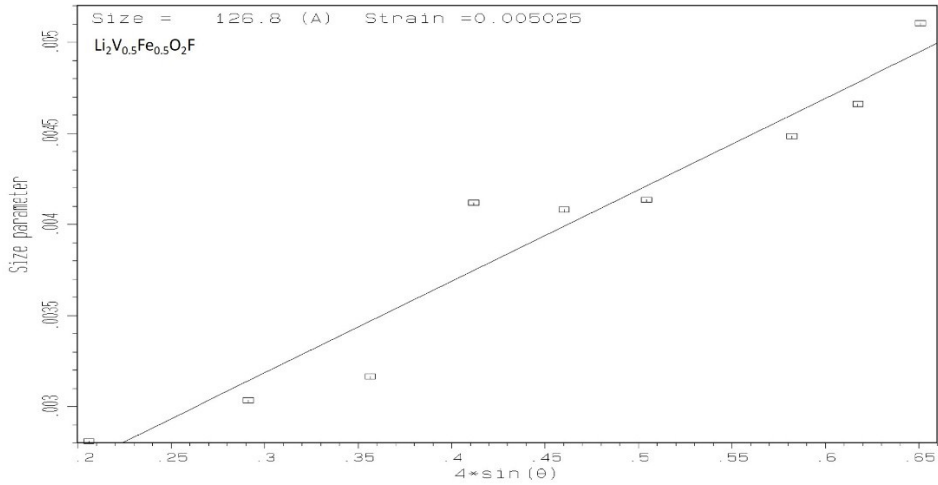
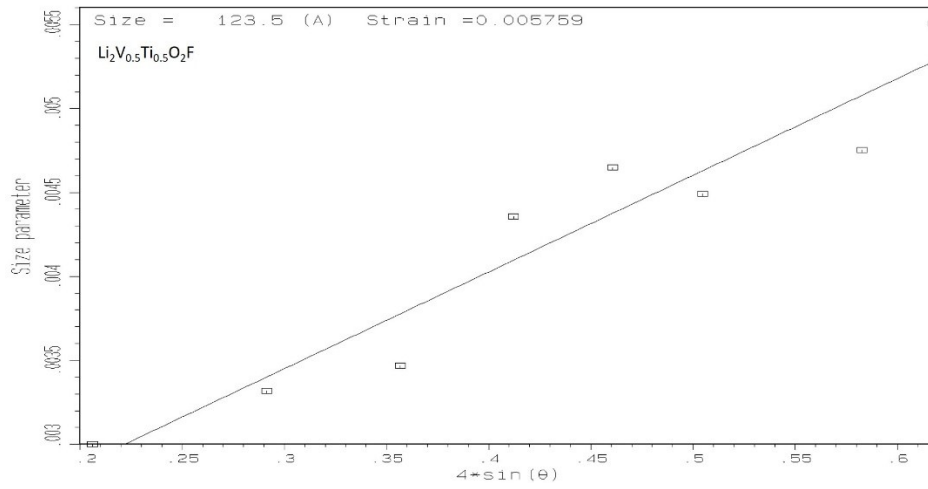
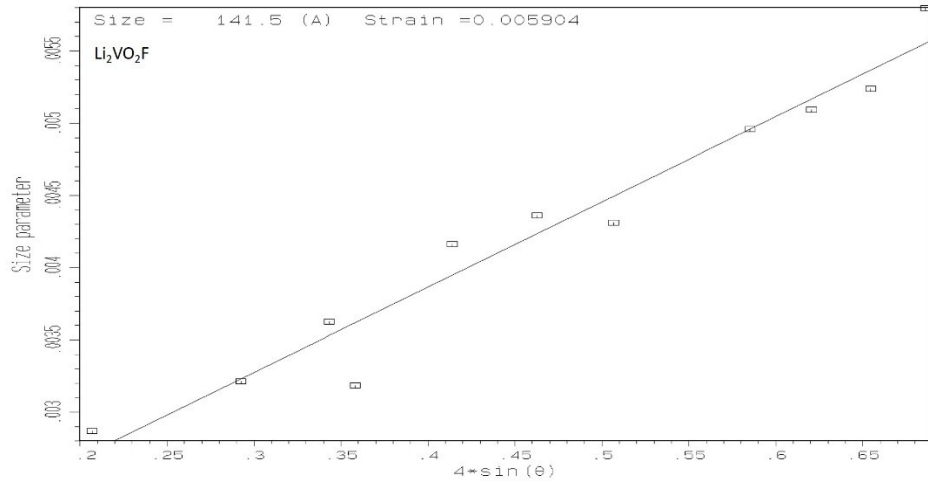
#Size and strain have been calculated with the Williamson-Hall Method using PowderPlot.³

³ PowderPlot written by Kenny Ståhl:

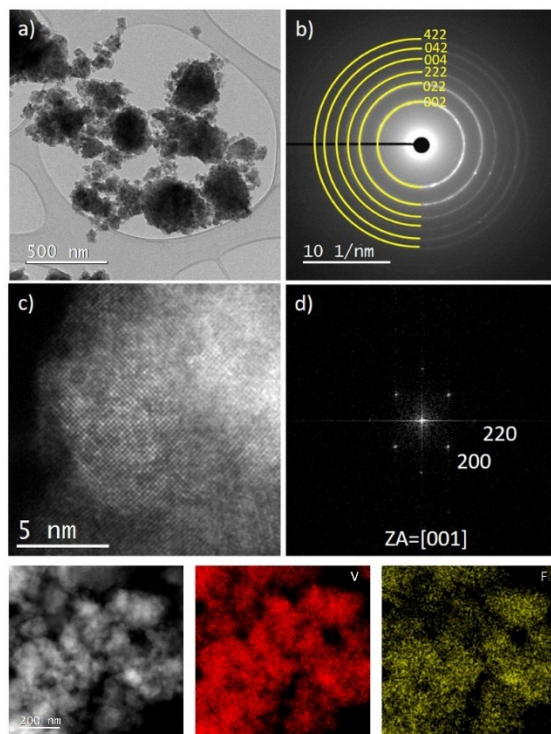
https://www.kemi.dtu.dk/english/research/physicalchemistry/protein_og_roentgenkrystallografi/computer_programs



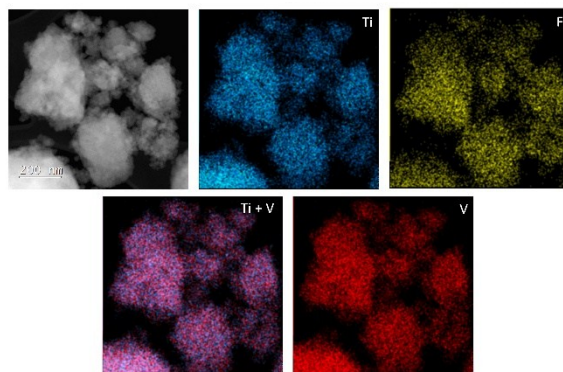
Supporting Information Figure S2: PXRD pattern of Li₂VO₂F with Rietveld refinement and Bragg positions of Li₂VO₂F, Si₃N₄ and V₂O₃. $\lambda = 0.21280 \text{ \AA}$.



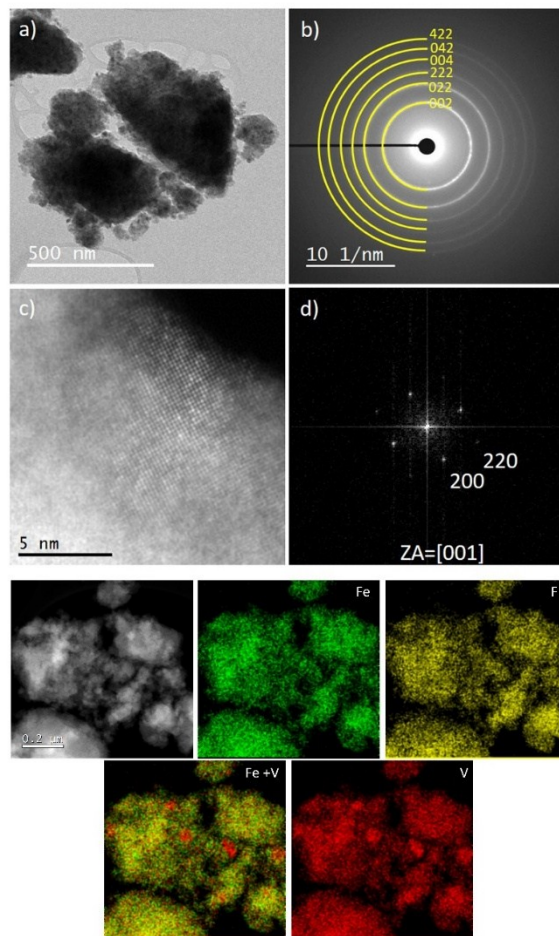
Supporting Information Figure S3: Williamson-Hall-Plot of $\text{Li}_2\text{VO}_2\text{F}$, $\text{Li}_2\text{V}_{0.5}\text{Ti}_{0.5}\text{O}_2\text{F}$ and $\text{Li}_2\text{V}_{0.5}\text{Fe}_{0.5}\text{O}_2\text{F}$.



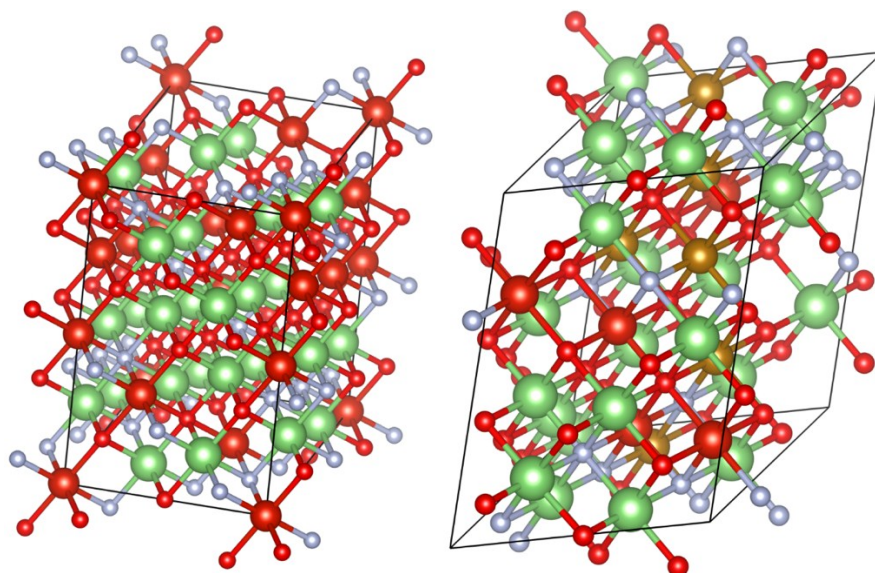
Supporting Information Figure S4: TEM analysis of $\text{Li}_2\text{VO}_2\text{F}$. a) TEM image and b) SAED pattern. c) High-resolution STEM ADF image with corresponding FFT d). Bottom: STEM ADF image and EDX elemental mapping of $\text{Li}_2\text{VO}_2\text{F}$ (the oxygen K_α map is not shown because of strong overlap with the vanadium L_α signal).



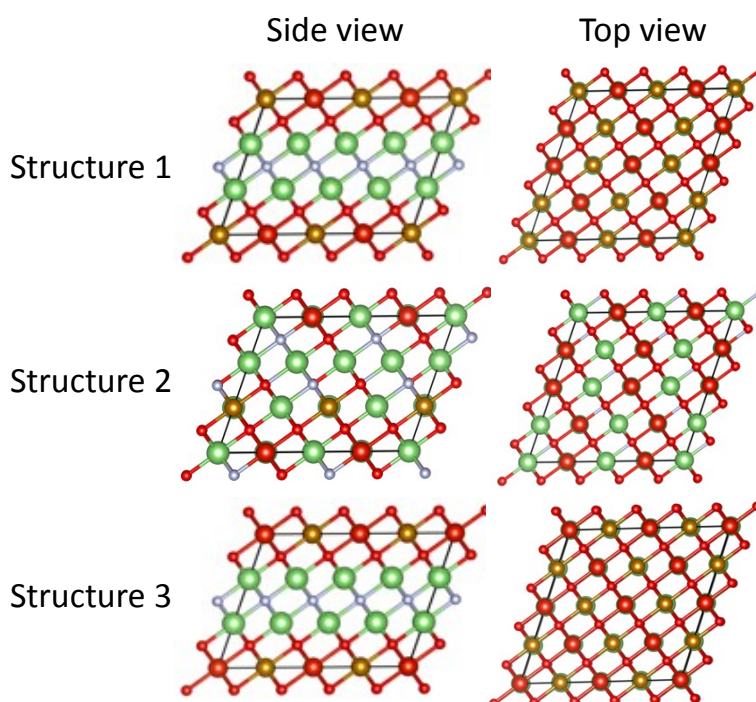
Supporting Information Figure S5: STEM ADF image and EDX elemental mapping of $\text{Li}_2\text{V}_{0.5}\text{Ti}_{0.5}\text{O}_2\text{F}$ (the oxygen K_α map is not shown because of strong overlap with the vanadium L_α signal).



Supporting Information Figure S6: TEM analysis of $\text{Li}_2\text{V}_{0.5}\text{Fe}_{0.5}\text{O}_2\text{F}$. a) TEM image and b) SAED pattern. c) High-resolution STEM ADF image with corresponding FFT d). Bottom: STEM ADF image and EDX elemental mapping of $\text{Li}_2\text{V}_{0.5}\text{Fe}_{0.5}\text{O}_2\text{F}$ (the oxygen K_α map is not shown because of strong overlap with the vanadium L_α signal).



Supporting Information Figure S7: Special Quasi-random Structures (SQS) of $\text{Li}_2\text{TMO}_2\text{F}$ (left) and $\text{Li}_2\text{TM}_{1.0.5}\text{TM}_{2.0.5}\text{O}_2\text{F}$ (right) with the cells containing 60 atoms.



Supporting Information Figure F8: Ordered structures of $\text{Li}_2\text{TM}_{1.0.5}\text{TM}_{2.0.5}\text{O}_2\text{F}$ derived from the $\alpha\text{-NaFeO}_2$ and $\gamma\text{-LiFeO}_2$ type oxide structures.

Supporting note 2 – relative stability of ordered and decomposed phase compared to disordered phase

The energy differences are computed using $\Delta E_{\text{ordered/decomposed}} = E_{\text{SQS}} - \min_{\text{ordered/decomposed}}(E_{\text{ordered/decomposed}})$, where $\min(E_{\text{ordered/decomposed}})$ corresponds to the minimum energy found in the ordered or decomposed phase.

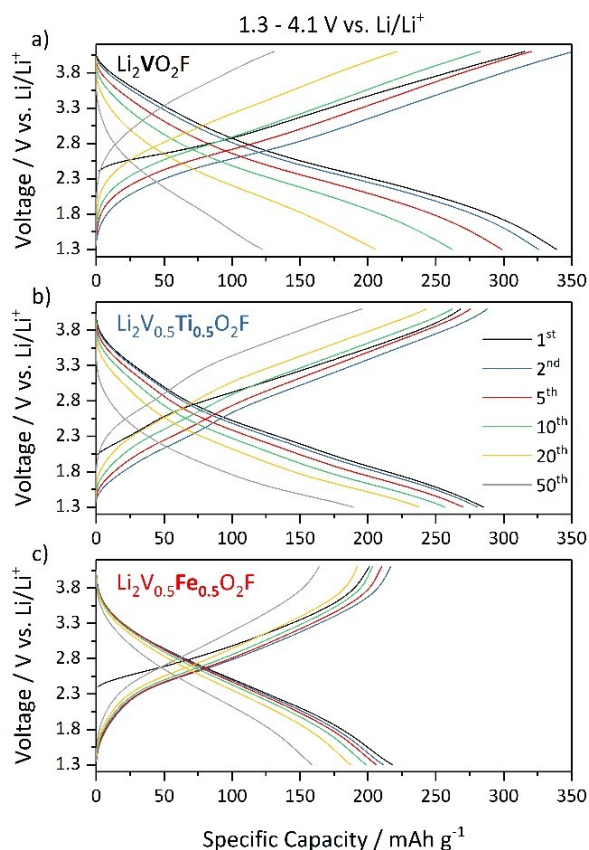
The SQS are shown in Figure S8, and the ordered structures include layered oxyfluoride structures and the structures derived from the α -NaFeO₂ and γ -LiFeO₂ type structures as shown in Figure S9. $\Delta E_{decomposed}$ is calculated using the decomposed product LiF + LiTMO₂ for Li₂TMO₂F and LiF + 0.5 LiTM1O₂ + 0.5 LiTM2O₂ for Li₂TM_{1.5}TM_{2.5}O₂F. The α -NaFeO₂ and γ -LiFeO₂ type oxide structures are considered, and the structure oxide yielding the lowest energy is chosen. $\Delta E_{ordered}$ and $\Delta E_{decomposed}$ are listed for all three compounds in Table S3.

Supporting information Table S2: Energy difference (in meV/atom) between ordered/decomposed state and disordered state.

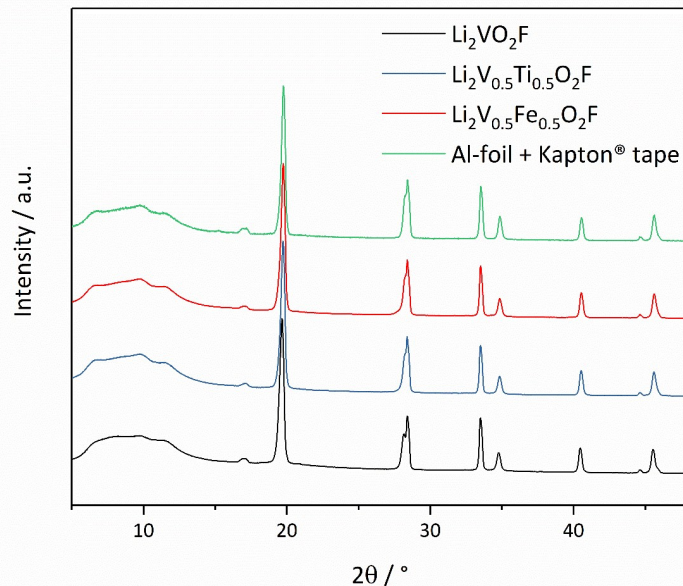
	$\Delta E_{ordered}$	$\Delta E_{decomposed}$
Li ₂ VO ₂ F	179	183
Li ₂ V _{0.5} Ti _{0.5} O ₂ F	144	147
Li ₂ V _{0.5} Fe _{0.5} O ₂ F	147	151

Supporting information Table S3: Oxidation states of TMs.

	Li ₂ VO ₂ F	Li ₂ V _{0.5} Ti _{0.5} O ₂ F	Li ₂ V _{0.5} Fe _{0.5} O ₂ F
SQS	V = {2+, 2+, 3+, 3+, 3+, 3+, 3+, 3+, 4+, 4+}	V = {3+, 3+, 3+, 2+, 2+}	V = {3+, 3+, 3+, 4+, 4+}
ordered	3+ for all V	3+ for all V and Ti	3+ for all V and Fe



Supporting Information Figure S9. Voltage profiles of a) Li₂VO₂F, b) Li₂V_{0.5}Ti_{0.5}O₂F and c) Li₂V_{0.5}Fe_{0.5}O₂F half-cells cycled within a potential range of 1.3 – 4.1 V vs. Li/Li⁺ with C/5-rate at 25 °C.

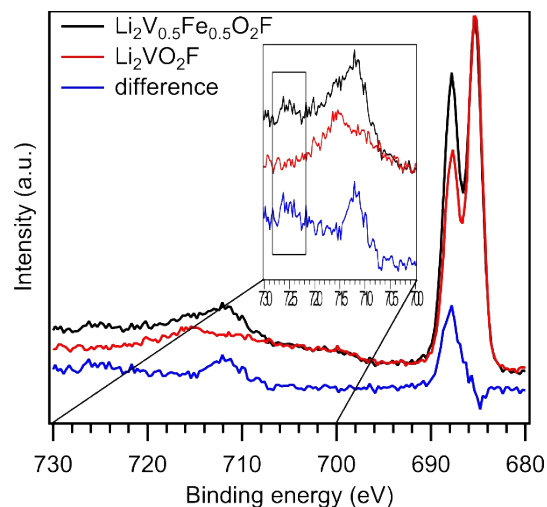


Supporting Information Figure S10: Ex-situ XRD pattern (Mo-K α 1) of the electrodes cycled after 100 cycles within a voltage range of 1.3–4.1 V vs. Li/Li⁺ at a rate of C/5. Reflections of the DRS phase is hidden by the reflections of the Al-foil current collector. However, no new reflections indicating new phases are present.

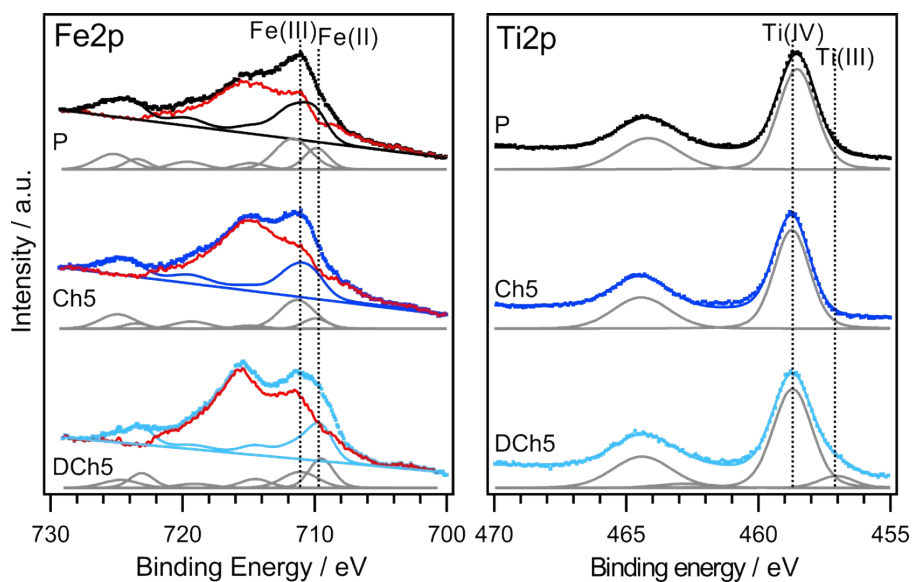
Supporting note 3 – Fe 2p peak fitting

Due to an overlap with the F 1s plasmon the Fe 2p contribution to the spectra is hard to distinguish. By comparing a survey of Fe-substituted and unsubstituted pristine material, it is seen that there is clearly an iron contribution, but that the Fe 2p_{3/2} contribution is hidden under the fluorine plasmon, see Figure S9. The Fe 2p_{1/2} on the other hand (~725 eV) lies above the fluorine plasmon and are therefore utilized for the fitting. The distances, peak widths and intensity ratios between the 2 p_{1/2}, 2 p_{3/2} and satellite are locked according to reference values for Fe²⁺ and Fe³⁺.⁴

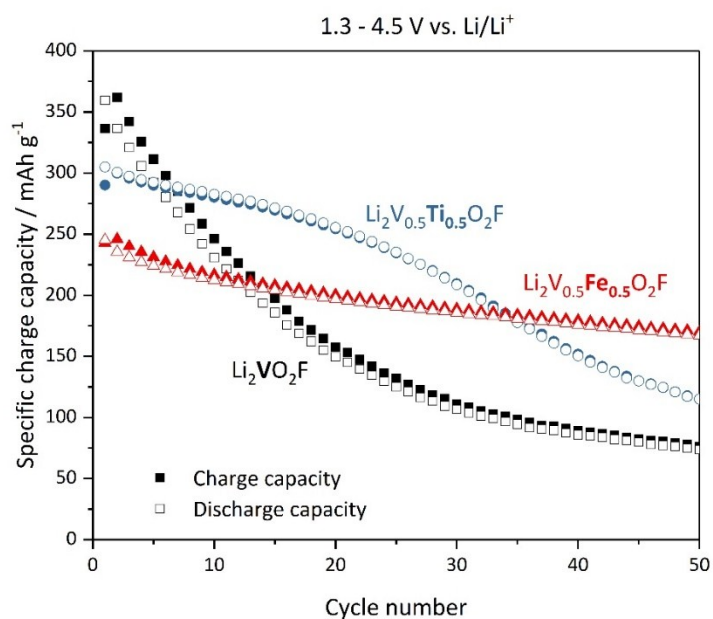
⁴ Lin, T.-C., Seshadri, G. & Kelber, J. A. A consistent method for quantitative XPS peak analysis of thin oxide films on clean polycrystalline iron surfaces. *Appl. Surf. Sci.* **119**, 83–92 (1997).



Supporting information Figure S11: Survey of $\text{Li}_2\text{V}_{0.5}\text{Fe}_{0.5}\text{O}_2\text{F}$ and $\text{Li}_2\text{VO}_2\text{F}$ as well as the difference between them. In the difference curve (blue) it is clearly seen that there is an iron signal. In the inset a zoom in of the Fe 2p region is shown. It can be seen that the fluorine plasmon overlaps with the Fe $2p_{3/2}$ peak but that the Fe $2p_{1/2}$ is at higher binding energies.



Supporting information Figure S12: Core level photoelectron spectra of Fe 2p and Ti 2p for the iron- and titanium substituted material, respectively. Dotted lines indicate reference values for different oxidation states.



Supporting Information Figure S13: Cycling performance (filled symbols: charge capacity, hollow symbols: discharge capacity of $\text{Li}_2\text{VO}_2\text{F}$ (black), $\text{Li}_2\text{V}_{0.5}\text{Ti}_{0.5}\text{O}_2\text{F}$ (blue) and $\text{Li}_2\text{V}_{0.5}\text{Fe}_{0.5}\text{O}_2\text{F}$ (red) as a function of cycle number for half-cells cycled within a potential range of 1.3 – 4.5 V vs. Li/Li⁺ with C/5-rate at 25 °C.